Practical considerations in using a binary pseudorandom array for instrument transfer function calibration

P. Z. Takacs[1*], S. Rochester[2], I. Lacey[3], K. Munechika[4], U. Griesmann[5], and V. V. Yashchuk[3]
[1]Surface Metrology Solutions LLC, 19 S 1st St, Unit B901, Minneapolis, MN 55401 USA,
[2]Rochester Scientific, LLC, 2041 Tapscott Avenue, El Cerrito, CA 94530, USA
[3]Advanced Light Source, LBNL, 1 Cyclotron Road, Berkeley, CA 94720, USA
[4]HighRI Optics, Inc., 5401 Broadway Terr, St. 304, Oakland, CA 94618, USA
[5]National Institute of Standards and Technology, Sensor Science Division, Gaithersburg, MD 20899, USA

ABSTRACT

Binary pseudo-random array (BPRA) artifacts are useful devices for calibrating the instrument transfer function (ITF) of interferometric microscopes and other optical and non-optical surface and wavefront measurement instruments. The intrinsic white noise character of the power spectral density function of the artifact simplifies the deconvolution of the ITF from the measured power spectral density (PSD). However, resampling of the BPRA intrinsic artifact features with the measurement tool's specific sampling pattern modifies the white noise character of the intrinsic spectrum and needs to be accounted for in the ITF-based data deconvolution process. We have developed an analytic solution to the spectrum of a resampled one- and two- dimensional BPRA. The resultant nominal PSD function is a simple two-parameter cosine function with a period equal to the resampled pixel width. A transfer function model for interferometric microscopes that incorporates this function, along with an ITF that includes aliasing effects and variable numerical aperture (NA), wavelength, and obscuration factor, is used to fit to the BPRA PSDs measured by an interference microscope for a range of objective and zoom lens magnification combinations.

Keywords: Instrument transfer function, ITF, metrology, standard calibration artifact, binary pseudorandom array, power spectral density, autocovariance

1. INTRODUCTION

Binary pseudo-random array (BPRA) artifacts [1-3] are useful in calibrating the instrument transfer function (ITF) of many precision metrology instruments, including phase-measuring interferometers and microscopes used to measure surface topography [4-11]. The binary height distribution of these artifacts has the mathematically useful property of having a white-noise power spectral density (PSD) over the spatial frequency range defined by the minimum feature size (MFS) and the total artifact size, which can be several thousand times the MFS. The flat white-noise spectrum makes it easy to deconvolve the ITF from the intrinsic BPRA spectrum. However, when a BPRA is actually used to calibrate an instrument, the intrinsic pattern features never align exactly with the boundaries of the camera pixels [12]. The BPRA features are resampled onto a grid defined by the magnified camera pixel array. This upsets the mathematically precise white-noise spectrum by introducing correlations between adjacent pixels in the measurement device. These correlations change the intrinsic flat white-noise PSD into a simple cosine function whose properties depend only on the ratio of the MFS to the magnified pixel size. The cosine function PSD can then be used to deconvolve the ITF from the measured PSD. We illustrate this by deconvolving BPRA artifact PSDs measured by an interference microscope with model microscope ITFs. The microscope model developed in an earlier paper [12] includes the resampled cosine PSD with adjustable parameters: numerical aperture, central obscuration, defocus, aliasing, and wavelength. The measurements are made on a 2D array artifact [13], and the average 1D PSD is computed by averaging the 1D PSDs computed from each row in the measured data. This effectively reduces a 2D problem to a 1D problem. We model the resampling of a 1D binary pseudo-random grating (BPRG) sequence by a detailed analysis of the autocovariance function (ACVF), averaged over subpixel shifts to account for non-isoplanatic nature of the digital imaging process.

*takacs.surfmetsoln@gmail.com; phone +1 631.833.0620

2. RESAMPLING

2.1 Base sequence definition

The BPRG used in the present simulations is an n=14,maximum length pseudo random sequence (MLPRS) with a cycle length of 2^n -1 = 16383 points, computed according to the method in Koleske and Sibener [2]. Each element is either a 1 or 0, and there is one more "1s" than there are "0s" for a duty cycle of effectively 50%. The mean of this sequence is 0.500031.. Subtracting this mean from each element, the root-mean-square value is exactly 0.500. This result is generally true for other binary pseudo-random sequences generated from other distributions as long as the duty cycle is near 50%. Figure 1 illustrates the first 50 points in the basic source sequence for n=14, along with its autocovariance function after subtracting the mean from each source element. We use the discrete ACVF as defined by Koleske[2] with an additional normalization factor

$$c_j = \frac{1}{N}\sum_{i=1}^{N} y_i y_{i+j} \tag{1}$$

which is a cyclic autocovariance where the y_{N+i} term is equal to y_i. There are always N terms in the sum, and the lag index, j, goes from 0 to N-1. The normalized ACVF consists of a single non-zero point at lag = 0 with all others reduced by a factor of N, which makes them essentially zero. The PSD computed from this mathematical sequence is a straight line, which is the characteristic of a white noise sequence. The single non-zero point at j = 0 in the ACVF confirms that this is indeed a white noise distribution. The value of the 0-lag point is the mean-square of the sequence. If the points in the sequence are scaled by some physical height value, Z, the mean value becomes Z/2 and the mean-square is $Z^2/4$ with the root-mean-square (RMS) equal to Z/2. The ACVF plot on the right in Fig. 1 is for the zero-mean sequence, where the mean value (almost exactly 0.500) is subtracted from each source point.

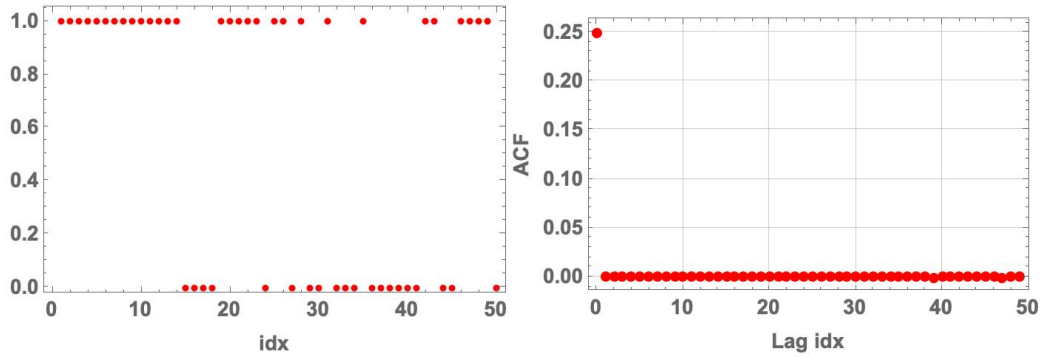

Figure 1- First 50 points in the BPRG sequence (left) and the corresponding ACVF (right) for parameters n=14 and M=1139. The ACVF has a single non-zero value at zero-lag, indicative of a white noise sequence. All others are reduced by a factor of N.

Actual BPRG artifacts are produced by a lithographic process where each feature is a multiple of some minimum feature size (MFS) [13]. The artifacts that we are simulating have a MFS of 400 nm. The features are arranged on a grid with a spacing of 400 nm. When we view these features through a microscope with a camera, the artifact's features are imaged onto the camera's pixel grid with some magnification factor. In general, the grid of the camera does not align perfectly with the grid of the BPRG. The case of oversampling was discussed in a previous paper [12]. Here we consider in more detail the case of undersampling, where the camera pixels are larger than the magnified BPRG MFS. When the MFS grid is undersampled, the signal recorded in each camera pixel combines the contributions of 2 or more adjacent features in the BPRG.

3. AUTOCOVARIANCE OF AN UNDERSAMPLED BPRG ARRAY

In the previous paper[12], simulations of PSDs and ACVFs computed from resampled 1D binary pseudo-random grating sequences led us to postulate that for undersampled data, where the resampling grid pixels are larger than the MFS of the BPRG, a simple two-parameter cosine function fits the computed 1D PSD:

$$S_1(f_x) = A + B\cos(2\pi D f_x) \quad \textbf{(2)}$$

where D is the resampled pixel size and f_x is the 1D spatial frequency. In the current paper, we confirm that this function is, indeed, the proper analytic solution to the resampling problem by deriving the results for A and B from an analysis of the autocovariance function. To achieve this result, we make use of the Wiener-Khintchine theorem [14] that connects the Fourier transform of the ACVF to the PSD of the sequence. For simplicity, we analyze the one-dimensional case for a BPRG sequence. Extension to the 2D case follows naturally and will be discussed in a future publication. We restrict the analysis to the undersampled case, where the resampled pixels are larger than the MFS. This insures that there will be no nulls in the PSD of the resampled data that will cause the MTF reconstruction function to blow up with divide-by-zero noise [12].

Complicating the analysis is the fact that sampling an image with a discrete array of pixels is a non-isoplanatic, non-shift-invariant process. The response of the system depends on the position of the image within a pixel [15, 16]. We employ the method in Park and Schowengerdt [17] that computes the ensemble average over all possible subpixel positions to define an average MTF for the non-isoplanatic system. Our analysis is valid for resampled pixels up to twice the base pixel size, i.e. for values of ε between 0 and 1, where ε is the fractional increase is size of the resampled pixel over the base minimum feature size. However, empirical results show that it is valid for all values of ε beyond 1. As shown in an earlier paper [12], it will be more convenient to express the final result for the A and B coefficients in terms of the ratio of the base MFS to the resampled pixels size, $k = d/D$. In this case, undersampled pixels have k-values that range from 1 to 0.

3.1 ACVF lag = 0 term, c_0

We start with an N-point random sequence of 1's and 0's that has a duty cycle of about 50 %. As discussed above, the statistics of this type of MLPRS sequence are such that the mean is 0.5 and the root-mean-square (RMS) is also 0.5. In the case of a physical realization of this sequence with features that have a height of Z, the mean and RMS are both equal to Z/2. Figure 2 illustrates the starting point for the analysis. The base BPRG features, with minimum feature size set to unity, are shown in blue, with values indicated by the x_i. The value of x_i is either 1 or 0, randomly distributed. The camera pixels, demagnified by projecting through the objective lens onto the BPRG, are shown in red, with values y_j. The width of each resampled pixel is given by the quantity 1+ε, where ε is the fractional increase in size over the base MFS. The value of y_i depends on the contributions from the base pixels that lie under it.

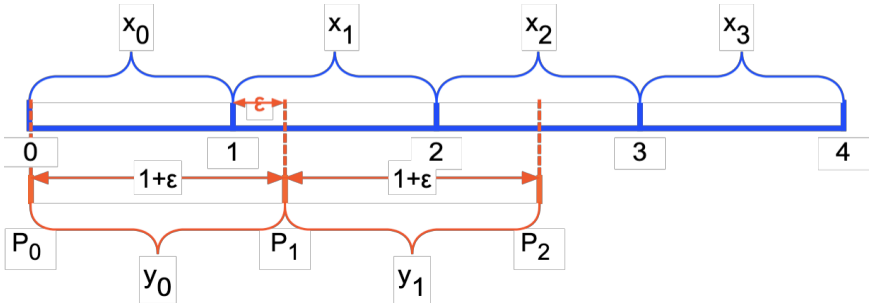

Figure 2 – Starting point for ACVF calculation. The source BPRG pixel grid is shown in blue; the resampled grid is in red. The value of each source pixel is x_i, that of the resampled pixels is y_j. The resampled pixels are larger than the MFS by the fraction ε.

With reference to Fig. 3, the first quantity that we need to compute is the ensemble average value for the autocovariance term with lag = 0, $c_0 = \langle y_0 y_0 \rangle$, averaged over all possible pixel shift values of P_0, e.g. for values of α between 0 and 1. Without loss of generality, we start with the two grids coincident at position 0. For this starting configuration, we see that the value of y_0 is given by an average of the value in x_0 and the fractional part in x_1:

$$y_0 = \frac{1}{1+\varepsilon}\left(x_0 + \varepsilon x_1\right) \quad (3)$$

Now we need to shift the resampled grid by a fractional distance, α, across the base pixel and see how each base x-pixel contributes to the resampled y-pixels. This results in a piecewise function defined by various breakpoints, as shown in Fig. 3. We notice that as α increases from 0 in Fig. 3(a), only the first 2 base pixels, x_0 and x_1, contribute to the y_0 value,

until the right side boundary of y_0, P_1, reaches a breakpoint at 2,in Fig. 3(b). This occurs when $\alpha = 1-\varepsilon$. For larger values of α, base pixel x_2 also contributes to the y_0 value in Fig. 3(c). So the expression for y_0 becomes a piecewise function of α:

$$y_0(\varepsilon,\alpha) = \begin{cases} \frac{1}{1+\varepsilon}\left[x_0(1-\alpha) + x_1(\varepsilon+\alpha)\right] & for\ 0 \le \alpha < 1-\varepsilon \\ \frac{1}{1+\varepsilon}\left[x_0(1-\alpha) + x_1 + x_2(\varepsilon+\alpha-1)\right] & for\ 1-\varepsilon \le \alpha \le 1 \end{cases} \tag{4}$$

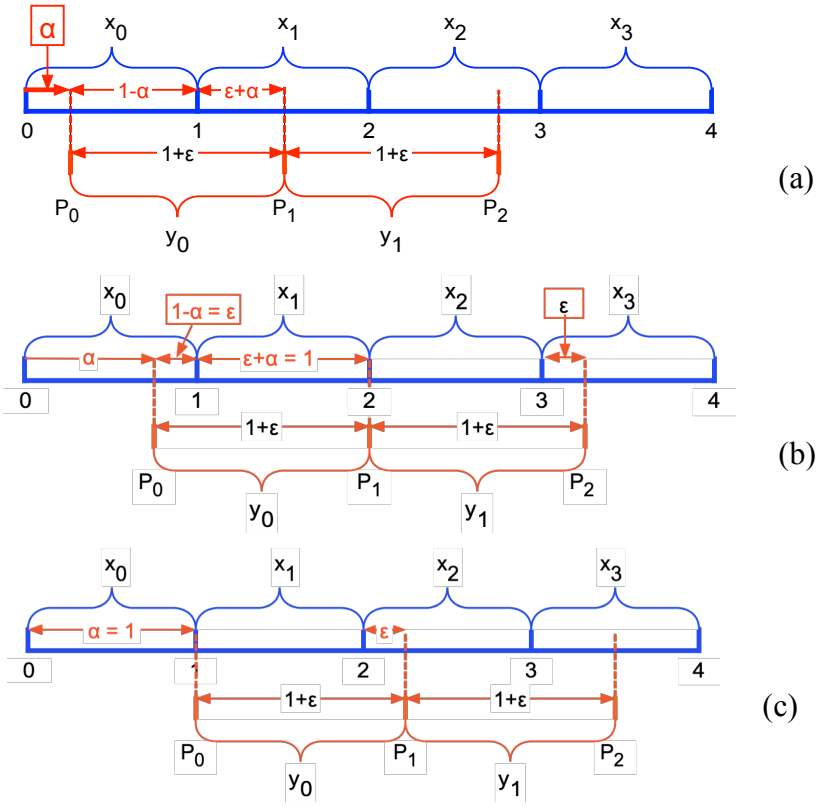

Figure 3 – Contributions of the x-pixels to y_0 as the resampled grid is shifted by α across the MFS pixel, x_0. (a) shows the shift of P_0 away from the initial position at 0 by a small fraction α. (b) shows the first breakpoint when P_1 reaches 2 when α = 1-ε. (c) shows the final configuration when P_0 reaches the right edge of base pixel x_0 for α = 1

We make use of a commercial mathematical analysis program to compute the expectation value $\langle y_0 y_0 \rangle$ as a function of ε and α and then average over all possible α values. Note that the product $\langle y_0 y_0 \rangle$ is the mean square of the resampled array, and is also the lag = 0 element of the autocovariance function. Performing the multiplications for the two piecewise elements, eliminating the cross terms whose expectation values are zero, and substituting in the $Z^2/4$ value for the $\langle x_i x_i \rangle$ terms, we get the following piecewise expression:

$$\langle y_0 y_0 \rangle_\alpha = \begin{cases} \frac{Z^2\left(1+2\alpha^2+2\alpha(\varepsilon-1)+\varepsilon^2\right)}{4(1+\varepsilon)^2} & for\ 0 \le \alpha < 1-\varepsilon \\ \frac{Z^2\left(3+2\alpha^2+2\alpha(\varepsilon-2)-2\varepsilon+\varepsilon^2\right)}{4(1+e)^2} & for\ 1-\varepsilon \le \alpha \le 1 \end{cases} \tag{5}$$

Now we average over all possible α values and end up with a single expression for the mean square of the y_0 term as a function of ε or k:

$$c_0 = \langle y_0 y_0 \rangle = \frac{Z^2(2+3\varepsilon)}{12(1+\varepsilon)^2} = \frac{1}{12} Z^2 k(3-k) \tag{6}$$

In Eq. (6) we have substituted in the value of k in terms of ε, where d is the base ground rule pixel size and D is the resampled pixel size:

$$k = \frac{d}{D} \text{ and } D = (1+\varepsilon)d = \frac{d}{k}$$
$$\therefore k = \frac{1}{1+\varepsilon} \text{ and } \varepsilon = \frac{1}{k} - 1 = \frac{1-k}{k} \tag{7}$$

Recall from above the c_0 is the mean-square of the resampled BPRG, so we can write the RMS of the resampled sequence in terms of the intrinsic feature height, Z:

$$rmsZ_k = Z\sqrt{\frac{k(3-k)}{12}} \tag{8}$$

Note that this RMS value is before the optical and pixel MTFs are applied. It is not what is seen in a measurement of the BPRA.

3.2 ACVF lag =1 term, c_1

In a similar way, we can compute the ensemble average of the lag =1 autocovariance term. This requires expressing the neighboring y_1 term as a function of α and ε. The piecewise functions now depend on the value of ε. As can be seen in Fig. 4 for $\varepsilon \le 0.5$, P_2 does not go beyond 4. So there are only 2 cases to consider for y_1: y_1A for $\varepsilon \le 0.5$, and y_1B for $\varepsilon > 0.5$.

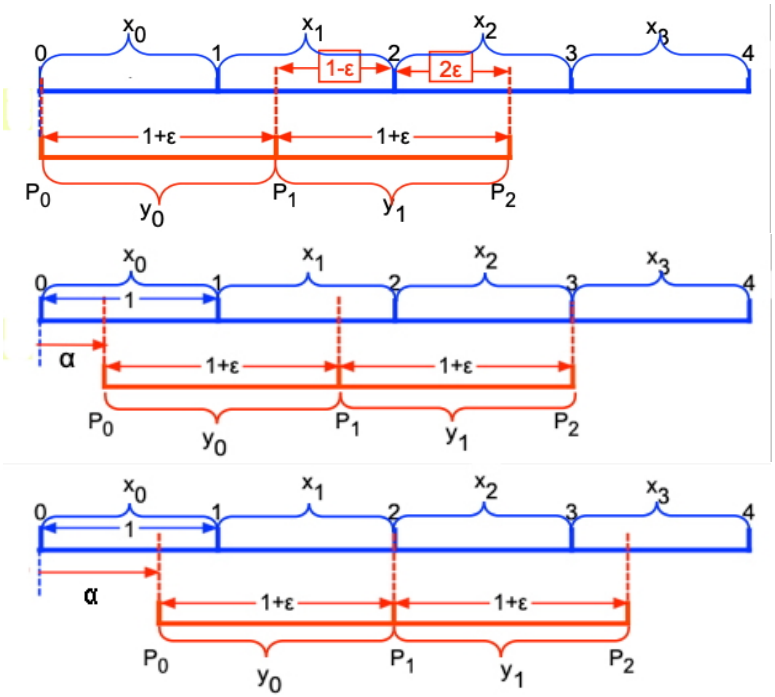

Figure 4 – Breakpoints for defining the piecewise function of α and $\varepsilon \le 0.5$ for case y_1A. P_2 does not go beyond 4 for this ε. (a) Starting configuration for α = 0. (b) First breakpoint when P_2 reaches 3. (c) Second breakpoint when P_1 reaches 2.

For y_1A with $\varepsilon \le 0.5$, there are 2 breakpoints in the piecewise function: the first when P_2 reaches 3, and the second when P_1 reaches 2. P_2 does not go beyond 4, so there is no x_4 contribution. The 3 piecewise components when $\varepsilon < 0.5$ are:

$$
\begin{aligned}
y1A1 &= \frac{1}{1+\varepsilon}\left[x_1\left(1-\varepsilon-\alpha\right)+x_2\left(2\varepsilon+\alpha\right)\right] && for\ 0 \le \alpha < 1-2\varepsilon \\
y1A2 &= \frac{1}{1+\varepsilon}\left[x_1\left(1-\varepsilon-\alpha\right)+x_2+x_3\left(2\varepsilon+\alpha-1\right)\right] && for\ 1-2\varepsilon \le \alpha < 1-\varepsilon \\
y1A3 &= \frac{1}{1+\varepsilon}\left[x_2\left(2-\varepsilon-\alpha\right)+x_3\left(2\varepsilon+\alpha-1\right)\right] && for\ 1-\varepsilon \le \alpha \le 1
\end{aligned}
\tag{9}
$$

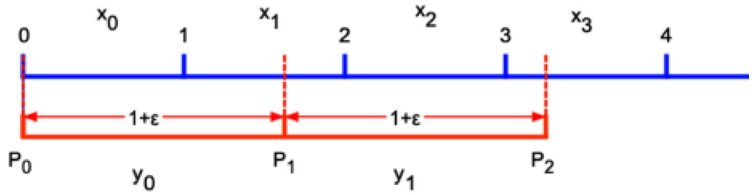

Figure 5 – Starting configuration for y_1B for $\varepsilon > 0.5$. For this case, P_2 does go beyond 4, so there is a contribution from x_4.

For $\varepsilon > 0.5$, the starting configuration for y_1B for $\alpha = 0$ is shown in Fig. 5. As α increases from 0, the breakpoints occur when P_1 reaches 2 and then when P_2 reaches 4. The piecewise contributions to y_1B are:

$$
\begin{aligned}
y1B1 &= \frac{1}{1+\varepsilon}\left[x_1\left(1-\varepsilon-\alpha\right)+x_2+x_3\left(2\varepsilon+\alpha-1\right)\right] && for\ 0 \le \alpha < 1-\varepsilon \\
y1B2 &= \frac{1}{1+\varepsilon}\left[x_2\left(2-\varepsilon-\alpha\right)+x_3\left(2\varepsilon+\alpha-1\right)\right] && for\ 1-\varepsilon \le \alpha < 2\left(1-\varepsilon\right) \\
y1B3 &= \frac{1}{1+\varepsilon}\left[x_2\left(2-\varepsilon-\alpha\right)+x_3+x_4\left(2\varepsilon-\alpha-2\right)\right] && for\ 2\left(1-\varepsilon\right) \le \alpha \le 1
\end{aligned}
\tag{10}
$$

The expressions for the $\langle y_0\ y_1\rangle$ expectations are more complicated now. When the piecewise expressions for y_0 are multiplied by the expressions for y_1 and the expectation values for the x-terms are substituted in, the result simplifies to

$$
\left\langle y_0 y_1 \right\rangle_\alpha = \frac{Z^2\left(\alpha-\alpha^2+\varepsilon-2\alpha\varepsilon-\varepsilon^2\right)}{4\left(1+\varepsilon\right)^2}
\tag{11}
$$

This expression for the expectation of the lag = 1 term is the same for both ε ranges. So we can integrate over α to get the average expectation as a function of ε, or k:

$$
c_1 = \left\langle y_0 y_1 \right\rangle = \frac{Z^2}{24\left(1+\varepsilon\right)^2} = \frac{k^2}{24}Z^2
\tag{12}
$$

The above analysis is tailored specifically to a BPRG that is a maximum length pseudo-random sequence (MLPRS) with specific statistical properties[2].The same analysis holds for other binary statistical distributions. However, the relation between the mean square and the peak-to-valley (PV) height of other distributions may not be the same as for the MLPRS. For this reason, the numerical factors in the c_0 and c_1 expressions may need to be adjusted.

4. PSD ANALYSIS

4.1 PSD from ACVF

Now that we have the analytic form of the ACVF terms for the resampled BPRG, we need to relate them to the parameters that describe the PSD for this sequence. From the definition of the cyclic ACVF in equation (1), we note that $c_j = c_{N-j}$ and, extending to negative lags, $c_{-j} = c_j$. For the resampled sequence, there are only 3 significant non-zero autocovariance coefficients; c_0, c_1, and c_{-1}, where $c_1 = c_{-1}$. Now we can apply the discrete form of the Wiener-Khintchine theorem [14] to compute the 2-sided PSD from the ACVF:

$$
S\left(f\right) = D\sum_{j=-\infty}^{\infty} c_j e^{-i2\pi fj} = D\left[c_0 + c_1\left(e^{-i2\pi f} + e^{i2\pi f}\right)\right] = D\left[c_0 + 2c_1\cos\left(2\pi f\right)\right]
\tag{13}
$$

where D is the resampled pixel width and f ranges from $-f_{Ny}$ to f_{Ny}, where the Nyquist frequency is given by $f_{Ny} = 1/2D$. The ideal PSD is a cosine function, as we surmised from earlier results [12]. In the form in Eq. (13), it is a 2-sided PSD, where the frequency encompasses both positive and negative frequencies. To be useful as input to the MTF model, the 2-sided PSD needs to be converted into the 1-sided form of equation (2) by folding the negative frequencies over into the positive frequencies. Because the 2-sided PSD of a real number sequence is symmetric about the DC term, folding amounts to doubling the coefficients of the positive frequencies and dropping the negative frequencies. Special consideration needs to be given to the Nyquist frequency point when the number of points in the input 1D array is even. In this case, the Nyquist point does not get doubled. The DC point never gets doubled. We then have for the 1-sided PSD

$$A_{1side} = 2c_0 D = 2c_0 \frac{d}{k}$$
$$B_{1side} = 4c_1 D = 4c_1 \frac{d}{k} \tag{14}$$

Substituting the values of c0 and c1 from equations (6) and (12), we get the cosine function coefficients in terms of the base BPRG parameters and the resampling factor, k:

$$A_{1side} = \frac{1}{6} Z^2 d\left(3 - k\right)$$
$$B_{1side} = \frac{1}{6} Z^2 d\, k \tag{15}$$

These analytic one-sided coefficients define the nominal PSD for a resampled BPRG artifact. As we will see in Sec. 5, it will be necessary to extend the valid frequency range beyond the Nyquist frequency to account for aliasing effects in actual measurements.

When we use the analytic expression for the PSD of a resampled BPRG in the MTF model, we normalize it to unity at $f = 0$ by dividing each coefficient by the sum of the two coefficients. The normalized coefficients take on a particularly simple form as a function of k:

$$A_{norm} = 1 - \frac{k}{3}$$
$$B_{norm} = \frac{k}{3} \tag{16}$$

We note that for undersampled pixels that become significantly larger than the base BPRA MFS, or conversely, when the BPRA MFS is smaller than the demagnified camera pixels, k approaches 0. In this case, the cosine function flattens out, becoming more white-noise-like. The high frequency content in the PSD is then limited by the resampled pixel size and cuts off well before the inherent BPRA limit. To optimize the ITF reconstruction process, we try to select a BPRA minimum feature size that is less than a factor of 2 smaller than the projected pixel size. This gives us maximum spatial frequency coverage over the BPRA bandwidth.

4.2 PSD of a resampled sequence: simulation

To illustrate the resampling process, we start with the BPRG shown in Fig. 1 and assign a base pixel width of 400 nm to each point. Then we resample onto a 450 nm grid. The k-factor for this simulation is 400/450 = 0.888. The resampled sequence and its ACVF are shown in Fig. 6 along with the 2-sided PSD computed from the resampled points. One can see that the regular pattern of 1's and 0's seen in Fig. 1 becomes a more randomized pattern owing to the averaging over adjacent pixels in the resampling process.

Note that the question about the randomness (uniformness) of the distribution of the shift values of a resampling process (assumed in the derivation of Eqs. (6) and (12)) directly relates to a more general mathematical question: "To what extent are arithmetical progressions of fractional parts stochastic?" [18]. An answer to this question is given in the so called 'Fractional Parts Equipartition Theorem' originally proved by H. Weyl in the beginning of the last century [19]. Weyl's Theorem states (in application to the resampling transformation problem formulated above) that the sequence of residues of an arithmetic progression, is statistically uniformly distributed if its steps D is incommensurable with d, which simply means that the ratio 1/k is irrational. However, it can also be shown to be approximately valid, for

example, empirically, for the case considered in this paper, where the shift values are uniformly distributed over the parameter α. A deeper discussion of this question is beyond the scope of the present paper and will be provided elsewhere.

The ACVF points show that only the lag 0 and lag 1 (and hence the lag N-1) terms are significantly greater than 0. The other lag terms are no longer constant, but have small values fluctuating around zero. This contributes to the noise seen in the periodogram estimate of the PSD points shown in red. However, when the noisy PSD is smoothed by applying a 10^{th} order Gaussian filter, the cosine function nature of the PSD becomes evident. When we fit the unfiltered points to the cosine function defined in Eq. (2), we get the curve plotted over the other two in the PSD frame. The values of the fit coefficients indicated on the plot are for the 2-sided PSD fit. When we double them for the 1-sided PSD, we get A_{fit} = 0.14214 and B_{fit} = 0.0573. Using the results of our analytic resampling analysis in Eq. (15), with Z = 1 and D = 0.400, the analytic values for ensemble average values of A and B are 0.1407 and 0.0592. The small differences between the analytic and fit coefficients are due to the fluctuations in the single realization of the ensemble.

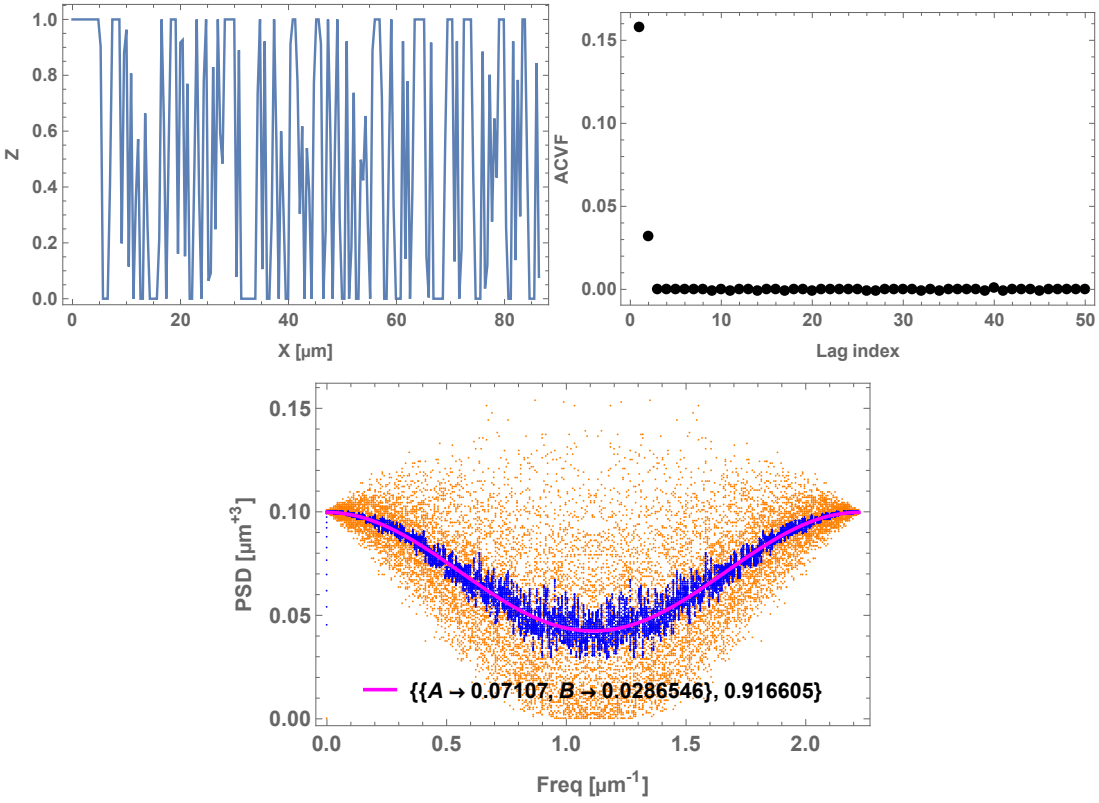

Figure 6 – (Top left) The first 100 points of a 400 nm BPRG resampled to a 450 nm grid. (Top right) The 50 initial lag points in the ACVF of the resampled sequence. The low-level points are no longer constant. (Bottom) 2-sided PSD computed from the sequence Z-values. The red points are the raw PSD values; the blue curve is smoothed by an order 10 Gaussian filter. The smooth curve is a fit of the raw points to an AB cosine function in the form of Eq. (2).

5. ITF MODEL WITH BPRA MEASUREMENTS

In the earlier paper [12], we modeled the ITF of a interferometric microscope as the product of the squares of the lens MTF and the pixel sampling MTF, with factors added for a central obscuration, defocus, and aliasing. We used this model to reconstruct the PSD of measurements of actual BPRA artifacts. At the time, we assumed that the spectrum of the BPRA was that of the ideal base array without any effects of resampling, i.e. a constant uniform horizontal line. As such, the ITF model did not fit the observed PSDs very well, especially at high frequencies for k-values close to 1. Now that we know how resampling affects the intrinsic spectrum of a measured BPRA, we can apply the ITF model to the measurements with improved results. The details of the ITF model for the interferometric microscope are presented in

the earlier paper[12] and will not be reproduced here. To summarize the process, we model the expected PSD that we should see for a given BPRA with a given microscope objective magnification and compare it to the measured PSD by dividing the measured by the model. Deviations from unity tell us how well our model describes our knowledge of the actual ITF. However, just removing the resampled BPRA PSD from the measured PSD gives the ITF, independent of any microscope model. Knowledge of this ITF will allow one to reconstruct the frequency content of objects viewed with this objective magnification combination.

The instrument used in the present work is a commercial optical surface profiler based on an interference microscope in the Advanced Light Source (ALS) X-Ray Optics Laboratory (XROL) [20]. This microscope has a 1200 x 1600 pixel camera with 8.68 µm square pixels, but the current measurements are analyzed on a 1000x1000 pixel subset grid. The nominal wavelength of the illumination system is 550nm. Each objective has a numerical aperture (NA) that, along with the wavelength, determines the maximum spatial frequency transmitted by the system, $f_{NA} = 2NA/\lambda$. The effective demagnification factor, given by the product of the objective magnification and the zoom lens parameter, determines the size of the camera pixels projected onto the BPRA object. We use demagnifications that provide projected pixel sizes that are greater than the MFS of the BPRA to insure that we are undersampling the artifact.

5.1 20x 1x with 0.4 µm BPRA

The averaged 1D PSD from the measurement of the 0.4 µm BPRA pattern with the 20x objective without additional zoom magnification is shown as the green curve in Figure The resampled pixel size for this measurement is 0.434 µm., and the k-factor is k = 0.922. The model MTF with the nominal NA and wavelength, and with no added obscuration, defocus, or aliasing factors, is shown in the plot on the left as the orange curve. The pixel sampling MTF is the topmost red curve and the lens MTF with no aliasing applied is the blue curve. The nominal lens cutoff frequency is 1.45 μm^{-1}, which is just beyond the Nyquist frequency, 1.15 μm^{-1}, so we expect a small amount of aliasing to be required. The ratio of the measured to modeled PSDs is shown in the points on the right. One can see that the ratio does not lie along a horizontal line at 1.0. The orange model MTF curve lies above the green measured PSD over the entire Nyquist frequency range. The dashed vertical red line indicates the Nyquist frequency for this resampled pixel size.

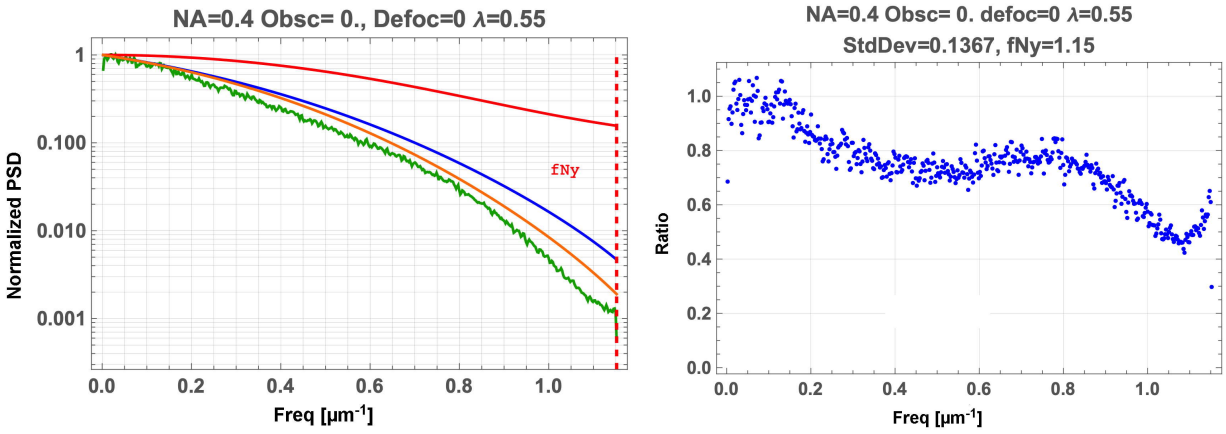

Figure 7 – (Left) 20x 1x measured PSD (green) with nominal model MTF (orange) without including the cosine function factor and aliasing effects. The red and blue curves are the MTF contributions of the pixel size and lens, respectively. (Right) Measured PSD normalized by the combined nominal lens (without any obscuration) and pixel sampling MTFs.

If we model this measurement without the cosine function PSD, i.e. with the flat, straight white noise PSD, the best we can do to fit the data is to add an obscuration fraction of 0.23 to the model, keeping NA = 0.4 and λ = 0.550 µm. This result from the previous work [12] is reproduced in Fig. 8. One can see that the "no resampling" model overestimates the ITF at high frequencies, so that the ratio drops significantly from unity.

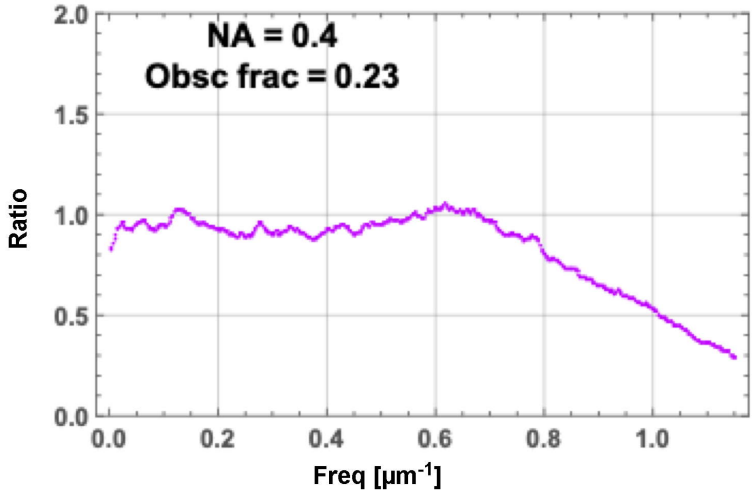

Figure 8 – Earlier result of ratio of measured PSD to modeled PSD without including the cosine function for the BPRA resampling, from [12]. The previous ITF model overestimates the ITF at high frequencies.

When we add aliasing to the model with the cosine function PSD and optimize the wavelength and obscuration parameters, we get a much better fit to the measured PSD, shown in Fig. 9. The parameter values after optimization are λ = 0.598 µm, obscuration fraction = 0.185, and NA = 0.4, with the lens cutoff frequency f_{lens} = 1.337 µm^{-1}. This is the best we can do for this objective-zoom combination. The small deviation from unity in the restored PSD is still not exactly a straight line, indicating our model is incomplete. However, if we just correct the measured BPRA PSD with the cosine function, we are left with the actual ITF of the microscope with this objective-zoom combination, which can then be used to restore the spatial frequency content of other observations.

Note that the optimized wavelength, 0.598 µm, differs from the nominal wavelength of the optical profiler, 0.550 µm. The source is a high intensity LED with a spectral bandwidth of 80 nm [21]. We allow wavelength to be an adjustable parameter since we do not know what the effective "average" wavelength will be after passing through the interferometer optics. The profiler is operated in coherence scanning mode, where the maximum of the envelope of the interference modulation determines the height in each pixel. For this reason, defocus is not considered in the model, as the surface is always in focus at the maximum modulation height.

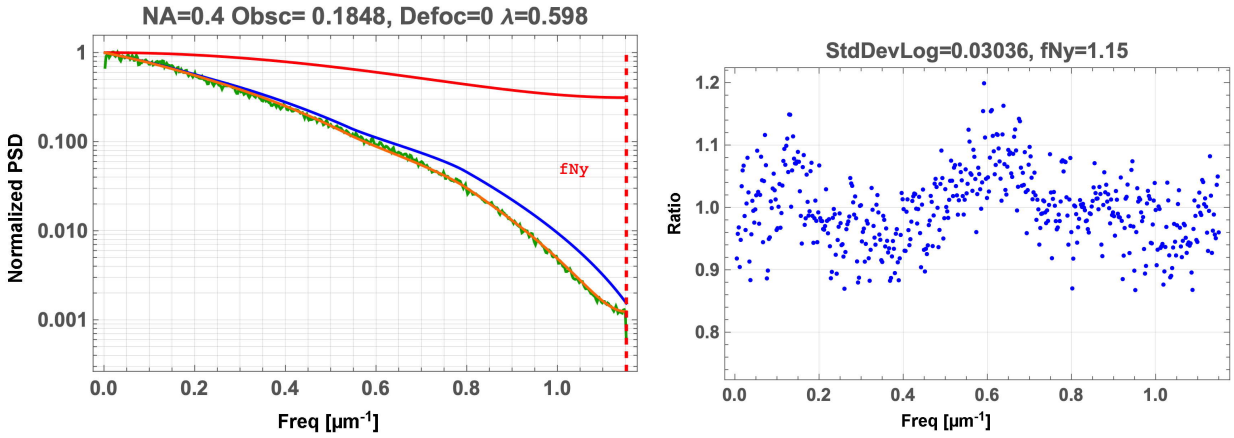

Figure 9 – The 20x 1x restored PSD after adding aliasing to the model and optimizing the wavelength and obscuration factor. The orange model curve is practically indistinguishable from the green measured PSD points. The measurement-to-model ratio (right) is now closer to unity over the full frequency range.

5.2 10x 1x with 0.4 µm BPRA

The 10x 1x magnification model components are shown in Fig. 10. The nominal PSD (magenta) is the cosine function appropriate for the k = 0.461 resampling, where the base BPRA MFS is 400 nm and the resampled pixel size is 868 nm. The MTFs for the pixel and lens attenuations are shown in red and blue. One can see that the lens cutoff extends almost out to twice the Nyquist frequency, so we expect aliasing to be a significant contribution to the model fit. The Nyquist frequency is 0.576 um^{-1} (red dashed line) and the lens cutoff is at 1.09 um^{-1} (blue dashed line).

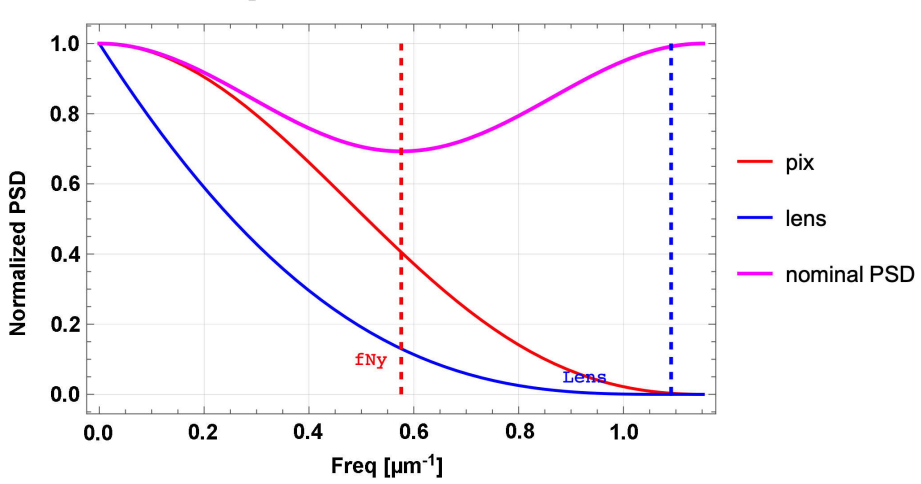

Figure 10 – 10x 1x model components for nominal starting parameters: NA = 0.30, λ = 0.550 µm, no obscuration, 400nm MFS and 868nm resampled pixel size. The nominal cosine PSD for k = 0.461 is shown as the magenta curve.

Figure 11 shows the model curve (orange) with the nominal microscope parameters. One can see that the model lies well above the measured PSD.

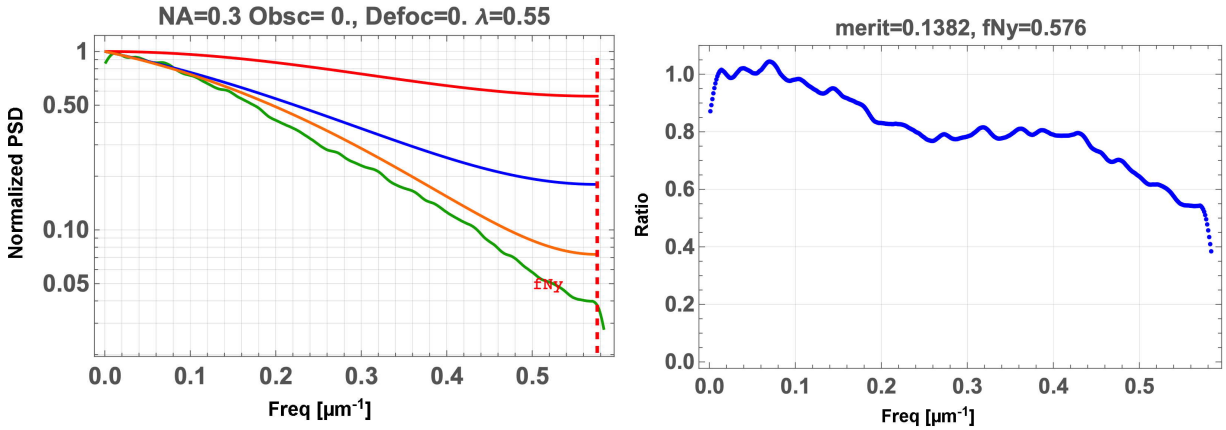

Figure 11 – {Left) 10x 1x measured PSD (green) with nominal MTF starting parameter curves. The lens MTF (blue curve on left) includes the aliased component. (Right) Ratio of measured-to-model PSDs for nominal starting parameters, showing the departure from unity over most of the frequency range.

When we optimize the fit parameters, we get the results shown in Fig. 12. The NA changes from 0.30 to 0.2641, the wavelength changes from 0.550 µm to 0.558 µm, and a slight amount of obscuration is added, 0.0137. The model curve (orange) now lies mostly on top of the measured PSD. However, the fit is not perfect, as shown by the departures from unity in the ratio curve in Fig. 12. The nature of the ratio curve is different from the 20x1x result in Fig. 9. This indicates again that our model does not include all the parameters necessary to fully describe the microscope ITF.

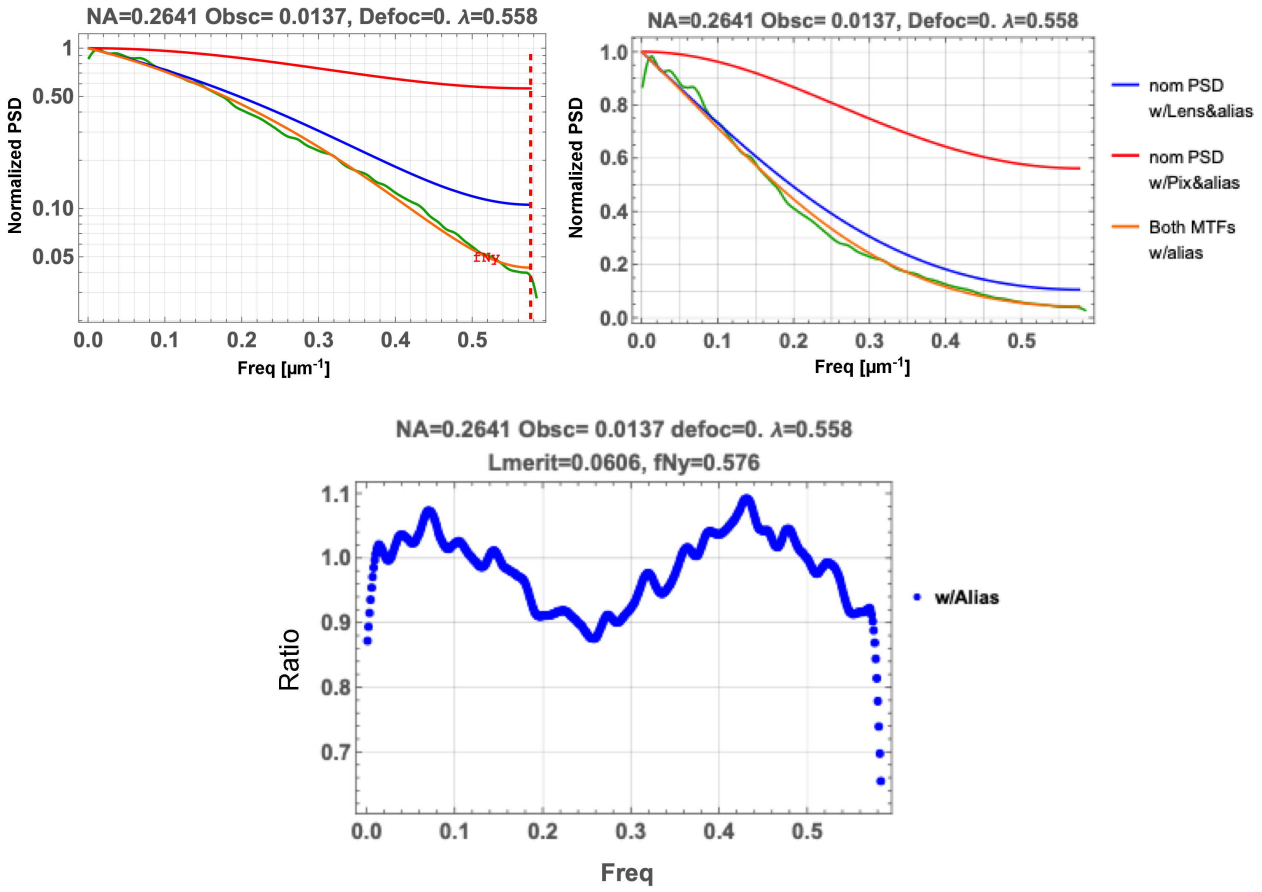

Figure 12 – 10x1x results after optimizing the model parameters. The model curve (orange) now lies mostly on top of the measurement PSD (green). The ratio of measurement-to-model in the bottom frame still shows departures from unity.

5.3 10x 2x with 0.4 µm BPRA

The 1x zoom configuration does not add an additional magnification element to the objective lens. The 2x zoom introduces an additional element into the optical path of the objective lens. For the 10x2x combination, the magnification is the same as for the 20x1x configuration. The resampled pixel size is 0.434 µm and k = 0.922. What differs from the 20x1x case is the NA: we assume the nominal NA should be the same as for the 10x1x case, NA = 0.30. This puts the lens cutoff frequency, 1.09 μm^{-1}, just before the Nyquist frequency, 1.15 μm^{-1}. The lens acts as a low pass filter in this case, so we get no aliasing of higher frequencies. We use the nominal NA, 0.30, along with the 0.550 µm wavelength and no obscuration as the starting point for the analysis. The model is shown with the measured PSD in Fig. 13. It is clear from the figure that the measured PSD has a cutoff frequency that is significantly lower than that of the nominal lens cutoff. The high frequency region of the measured PSD appears to drop off into the noise level. We need to modify the analysis to remove the noise and limit the model fitting to the region below the redefined lens cutoff frequency that depends on a variable NA and wavelength.

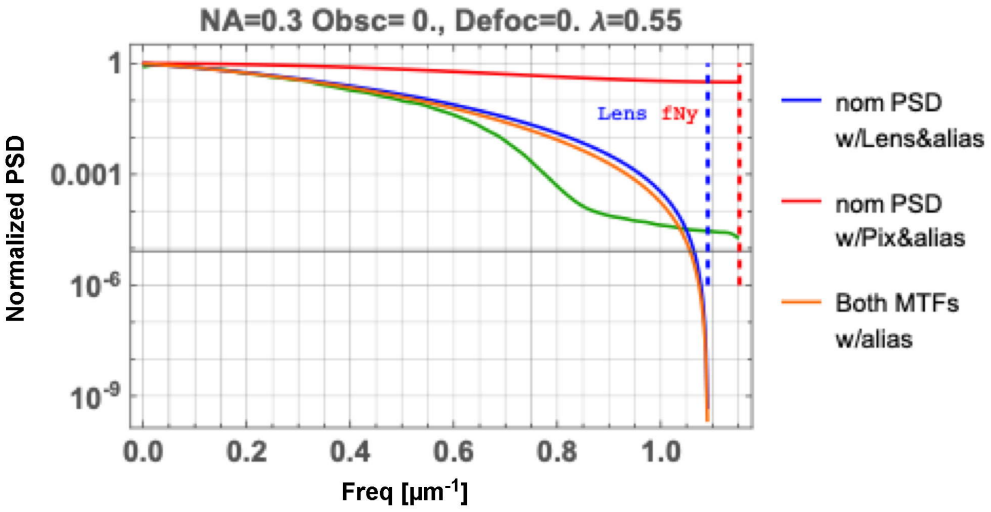

Figure 13 – Model fit to the nominal parameters for the 10x2x magnification combination. The actual lens cutoff appears to be at a significantly lower frequency than nominal.

Figure 14 shows the baseline-subtracted measured PSD curve for the 10x2x case. This serves as the starting point for the modeling. We need to adjust the NA and wavelength to match the observed cutoff frequency.

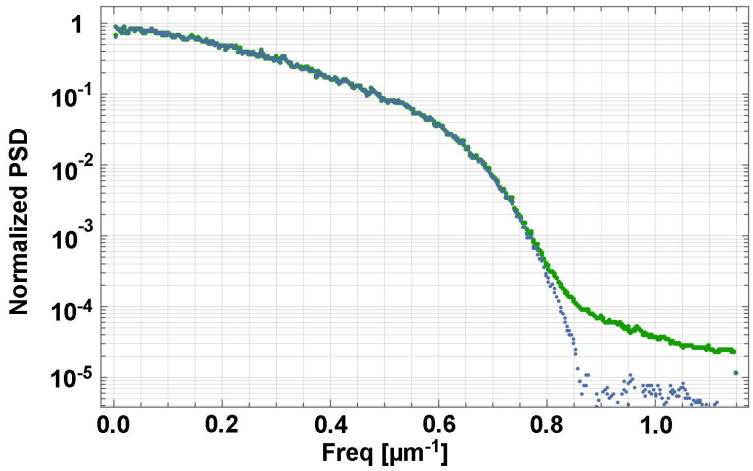

Figure 14 – The blue points are the result of subtracting a constant baseline level from the measured green curve.

The optimized parameters that produce the best fit shown in Fig. 15 are NA = 0.234, λ = 0.524 μm with no obscuration. The cutoff frequency is now 0.893 μm^{-1}, significantly lower than the expected 1.09 μm^{-1}. The ratio of measured-to-model PSDs on the right in Fig. 15 indicates that the model underestimates the measured PSD over most of the range. But some of this may arise from uncertainty in how the low frequency region is normalized because of the unusual low frequency behavior of the measured PSD, as seen in the upper right frame of Fig. 15. In any case, the BPRA measurement clearly shows the deviation of the actual ITF from the nominal ITF for this magnification combination. Why the model results for the 10x objective NA and the lens cutoff frequency with the 2x magnification zoom differ so much from the nominal values remains unclear.

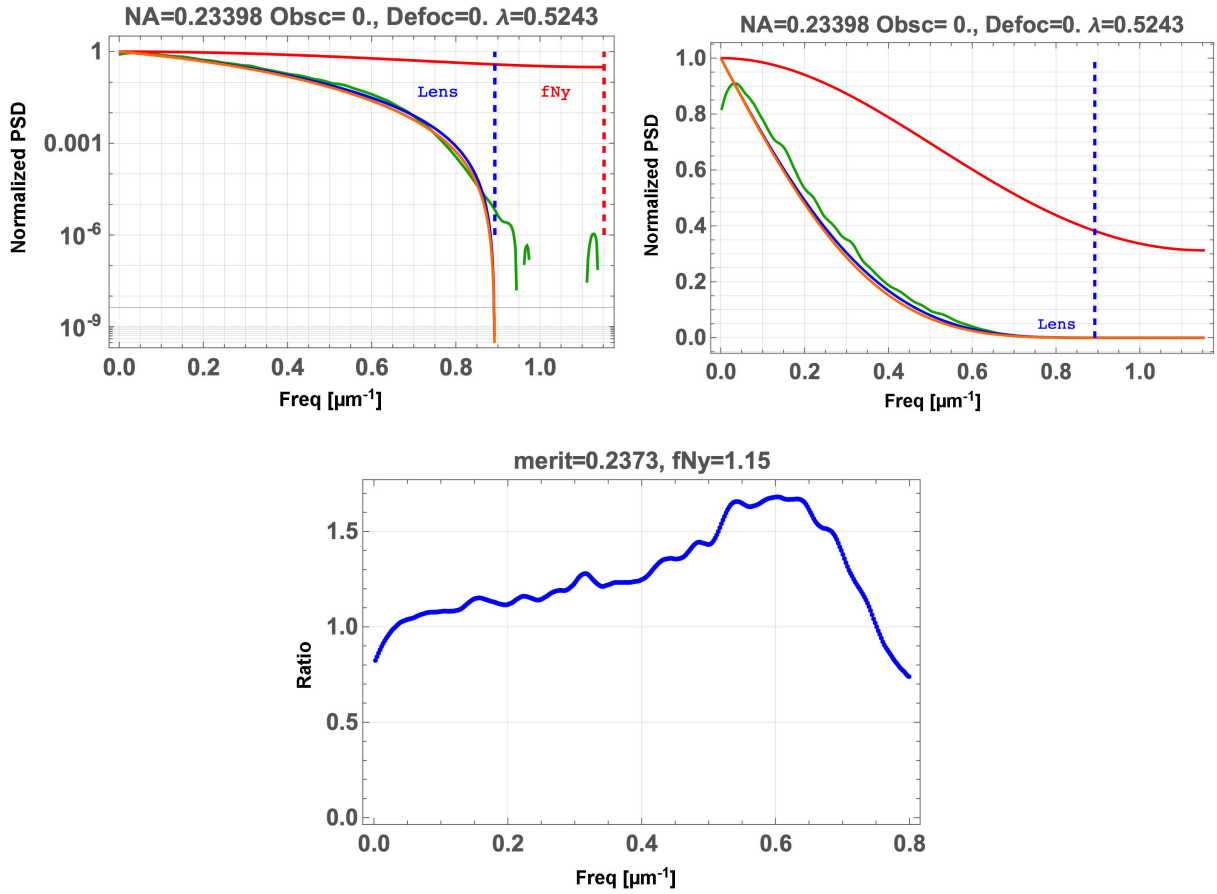

Figure 15 – Model curves fit to the 10x2x measured PSD (green). The fit is restricted to the frequency range below the apparent cutoff at 0.893 μm^{-1} after the baseline is subtracted. The model fit for this magnification combination with the 2x zoom added is not as good as for the others without the zoom lens.

6. CONCLUSION

Binary pseudo-random array artifacts have been shown to be useful in measuring the ITF of a multitude of metrology instruments. However, the theoretical white-noise spectrum of the intrinsic array needs to be modified when employed in systems that image the base artifact onto a grid with pixels larger or smaller than the minimum feature size of the artifact. We have shown that for undersampling, where the resampled pixels are larger than the base MFS, the intrinsic artifact white noise spectrum becomes a simple cosine function. The measured spectrum of an artifact can then be normalized by the cosine function appropriate for the resampling parameter, k, which then results in the ITF of the instrument. This microscope model with this modified BPRA PSD appears to fit some of the interferometric microscope measurements well with adjustments to some of the parameters. Other objective combinations require significant adjustments. Deviations in the measured-to-model PSDs indicate that we have not included all parameters in the model that affect the complete ITF.

ACKNOWLEDGEMENTS

This work was supported in part by the U.S. Department of Energy Office of Science, Office of Basic Energy Sciences, and Small Business Technology Transfer (STTR) programs under Award Numbers DE-SC0011352, DE-SC0022373, and DE-SC0022412 to HighRI Optics, Inc. and Rochester Scientific, LLC. It was also supported by the U.S. NASA STTR program under Contracts #80NSSC20C0505 and #80NSSC22PB039 to HighRI Optics, Inc. Research at the

Advanced Light Source at Lawrence Berkeley National Laboratory are supported by the Office of Science, Office of Basic Energy Sciences, and Material Science Division of the U.S. Department of Energy under Contract No. DE-AC02-05CH11231. Surface Metrology Solutions LLC acknowledges support from the Regents of the University of California under subcontracts #7528983 and #7647045.

DISCLAIMER

REFERENCES

[1] E. E. Fenimore, and T. M. Cannon, "Coded aperture imaging with uniformly redundant arrays," Applied Optics, 17 (3), pp. 337-347 (1978) doi: 10.1364/AO.17.000337

[2] D. D. Koleske, and S. J. Sibener, "Generation of pseudorandom sequences for use in cross-correlation modulation," Rev. Sci. Instrum., 63 (8), pp. 3852-3855 (1992)

[3] V. Yashchuk, S. Babin, S. Cabrini *et al.*, "Characterization and operation optimization of large aperture optical interferometers using binary pseudorandom array test standards", in *Interferometry XIX*, Proc. SPIE **10749,** (2018) 10.1117/12.2322011

[4] V. V. Yashchuk, W. R. McKinney, and P. Z. Takacs, "Binary pseudorandom grating standard for calibration of surface profilometers," Optical Engineering, 47 (7), pp. 073602 (2008) doi: 10.1117/1.2955798.

[5] V. V. Yashchuk, W. R. McKinney, and P. Z. Takacs, "Binary pseudo-random grating as a standard test surface for measurement of modulation transfer function of interferometric microscopes", in *Advances in Metrology for X-ray and EUV Optics II*, Proc. SPIE **6704,** (2007)

[6] V. V. Yashchuk, S. Babin, S. Cabrini *et al.*, "Binary pseudorandom array test standard optimized for characterization of large field-of-view optical interferometers", in *Interferometry XX*, Proc. SPIE **11490,** pp. 30 (2020) 10.1117/12.2568309

[7] V. V. Yashchuk, R. Conley, E. H. Anderson *et al.*, "Characterization of electron microscopes with binary pseudo-random multilayer test samples," Nuclear Instruments & Methods in Physics Research Section a-Accelerators Spectrometers Detectors and Associated Equipment, 649 (1), pp. 150-152 (2011) doi: 10.1016/j.nima.2010.11.124

[8] V. V. Yashchuk, E. H. Anderson, S. K. Barber *et al.*, "Calibration of the modulation transfer function of surface profilometers with binary pseudorandom test standards: expanding the application range to Fizeau interferometers and electron microscopes", in *Optical Engineering*, Proc. SPIE **50,** (2011)

[9] V. V. Yashchuk, E. H. Anderson, S. K. Barber *et al.*, "Calibration of the modulation transfer function of surface profilometers with binary pseudo-random test standards: Expanding the application range", in *Advances in Metrology for X-Ray and EUV Optics III*, Proc. SPIE **7801,** (2010) 10.1117/12.860049

[10] S. K. Barber, E. D. Anderson, R. Cambie *et al.*, "Binary pseudo-random gratings and arrays for calibration of modulation transfer functions of surface profilometers," Nuclear Instruments & Methods in Physics Research Section a-Accelerators Spectrometers Detectors and Associated Equipment, 616 (2-3), pp. 172-182 (2010) doi: Doi 10.1016/J.Nima.2009.11.046

[11] V. V. Yashchuk, W. R. McKinney, and P. Z. Takacs, "Test surfaces useful for calibration of surface profilometers", Patent #8,616,044,USA, Mar 21, 2008

[12] P. Z. Takacs, S. Rochester, I. Lacey *et al.*, "Calibration, modeling, parameterization, and verification of the instrument transfer function of an interferometric microscope", in *Interferometry XXI*, Proc. SPIE **12223,** pp. 1222308 (2022) 10.1117/12.2633116

[13] K. Munechika, W. Chao, S. Dhuey *et al.*, "Binary pseudo-random array standards for calibration of 3D optical surface profilers used for metrology with aspheric x-ray optics", in *Interferometry XXI*, Proc. SPIE **12223,** pp**.** 1222307 (2022) https://doi.org/10.1117/12.2633163

[14] J. S. Bendat, and A. G. Piersol, [Random Data: Analysis and Measurement Procedure], John Wiley & Sons, New York (1986).

[15] W. Wittenstein, J. C. Fontanella, A.R.Newbery *et al.*, "The definition of the OTF and measurement of aliasing for sampled imaging systems," Optica Acta*,* 29 (1), pp. 41-50 (1982)

[16] ISO, 15529:2010 - Optics and photonics — Optical transfer function — Principles of measurement of modulation transfer function (MTF) of sampled imaging systems] *International Organization for Standardization*, Geneva (2010).

[17] S. K. Park, and R. A. Schowengerdt, "Image sampling, reconstruction, and the effect of sample-scene phasing," Applied Optics*,* 21 (17), pp. 3142-3151 (1982)

[18] V. I. Arnol'd, "To what extend are arithmetical progressions of fractional parts stochastic?," Russian Math. Surveys*,* 63 (2), pp. 205-220 (2008) doi: 10.1070/RM2008v063n02ABEH004514.

[19] H. Weyl, "Über die Gleichverteilung von Zahlen mod. Eins," Mathematische Annalen LXXVII, pp. 313-352 (1916)

[20] V. V. Yashchuk, N. A. Artemiev, I. Lacey *et al.*, "A new X-ray optics laboratory (XROL) at the ALS: Mission, arrangement, metrology capabilities, performance, and future plans", Proc. SPIE **9206,** pp**.** 92060I/1-19 (2014) 10.1117/12.2062042

[21] L. Deck, and C. Evans, "High performance Fizeau and scanning white-light interferometers for mid-spatial frequency optical testing of free-form optics", in *Advances in Metrology for X-Ray and EUV Optics*, Proc. SPIE **5921,** pp**.** 59210A (2005) 10.1117/12.616874